Chapter 6
Damage Identification Strategy in Time-Varying Dynamic Systems Combining Cepstral and Image-Based Features

Sina Shid-Moosavi, Costanza Speciale, and Eleonora Maria Tronci

Abstract Damage identification and performance assessment in structural systems are vital for ensuring their safety, durability, and efficiency. Vibration-based pattern recognition strategies have become popular in the past decades to identify anomalies using the vibration response from the monitored structures. However, conventional methodologies often fail to recognize and classify the different types of damage, particularly in dynamic structural environments where patterns change over time. These limitations highlight the need for a more adaptive and comprehensive approach that can adjust to time-evolving conditions and detect subtle variations indicative of damage. This study aims to develop an innovative framework for damage identification by integrating cepstral and time-image-based features to leverage the strength of both sets of indicators. Time image-based features like the Gramian Angular Field capture underlying structural dynamics by encoding temporal correlations among data points as angular values in a polar coordinate system. This technique allows for the application of image-based machine learning methods to time-series analysis by converting the data into a two-dimensional matrix. Additionally, combining cepstral coefficients improves the capability of tracking stationary and nonstationary changes in the frequency content of the systems. By fusing these sets of parameters, this study aims to enhance the accuracy and efficiency of structural damage identification, particularly in systems with time-varying behaviors.

Keywords Damage Identification · Pattern Recognition · Structural Health Monitoring · Cepstral Coefficient · Gramian Angular Fields

Introduction

Vibration-based Structural Health Monitoring (SHM) aims to develop reliable methods for detecting damage by evaluating changes in the vibration responses of civil structures [1, 2]. In this context, structural damage is typically defined as any alteration in a system's material or geometric properties, such as boundary conditions or connectivity, that negatively impacts its performance, both in the present and the future, and ultimately modifies its dynamic response [3]. To identify these changes, SHM often employs Pattern Recognition techniques, which focus on detecting significant variations in parameters that characterize a structure's behavior and health. These parameters, known as Damage Sensitive Features (DSFs), provide a basis for assessing the condition of the monitored system [4].

However, applying these techniques to large-scale, complex, and time-varying systems, such as those found in civil, mechanical, and aerospace engineering, presents numerous challenges. These challenges arise from factors like the scale of the structure, variability in support conditions, sensor noise, limited sensor coverage, and fluctuations in operational loads [5]. The ability to accurately detect damage under such conditions is highly dependent on the selection of effective DSFs, features that must be responsive to structural changes while remaining resilient to external and operational influences and characterized by an easy and user-independent extraction process.

Various parameters have been proposed as DSFs, each with strengths and weaknesses. Modal parameters, like natural frequencies and mode shapes, are widely used due to their connection to structural stiffness and spatial information [6].

Sina Shid-Moosavi · Eleonora Maria Tronci
Department of Civil and Environmental Engineering, Northeastern University, Boston, MA, USA
e-mail: shidmoosavi.s@northeastern.edu; e.tronci@northeastern.edu

Costanza Speciale
Department of Mechanical and Aerospace Engineering, Sapienza University of Rome, Rome, Italy
e-mail: speciale.1836174@studenti.uniroma1.it

Matthew Whelan et al. (eds.), *Dynamics of Civil Structures, Vol. 2*, Conference Proceedings
of the Society for Experimental Mechanics Series, https://doi.org/10.13052/97887-438-0147-4_6

However, they are sensitive to environmental and operational variations, and their extraction is computationally intensive, often relying on user expertise, which limits their use in real-time, dynamic monitoring [7].

This research begins by leveraging cepstral coefficients as damage-sensitive features, which offer a compact and computationally efficient way to capture the spectral content of a system's dynamic response. Initially developed for speech recognition, cepstral coefficients have recently gained traction in structural damage detection [8, 9], thanks to their ability to track both stationary and nonstationary changes in frequency content [10], thereby improving robustness in identifying damage under varying conditions. However, relying solely on cepstral features may not fully capture the complexity of damage patterns in dynamic environments, especially when the system's behavior evolves over time. While cepstral coefficients are effective in capturing the spectral characteristics of dynamic systems, they provide a single-window representation of the system's behavior. This means that although they offer insight into the overall frequency content, they aggregate the response over the window's duration, making it difficult to pinpoint the exact moment when damage occurs within that window. Consequently, this can limit the ability to detect complex, evolving damage patterns, especially when damage manifests as a brief or subtle change within the time window. The inability to precisely localize the damage event within the window motivates the need for additional features that can capture both the temporal evolution of the system and the finer, more complex patterns of damage across time.

To address the limitation of cepstral coefficients' single-window representation, this work introduces a novel framework that combines them with time-image-based features, specifically the Gramian Angular Field (GAF). GAF transforms time-series data into two-dimensional images, capturing temporal correlations by encoding data points as angular values in a polar coordinate system [11]. This allows for a finer resolution of the temporal dynamics, complementing the cepstral coefficients' ability to track stationary and nonstationary frequency content changes. By merging these two techniques, this approach enhances the robustness and accuracy of damage identification, particularly in dynamic environments where damage patterns evolve over time and require precise localization [10, 12].

The novelty of this framework lies in its ability to merge two complementary feature types: cepstral coefficients provide valuable insight into the system's spectral properties, while GAF captures the temporal evolution of vibration signals in a format that can be analyzed using advanced machine learning techniques. This dual-feature approach enables a more comprehensive analysis of the system's behavior, especially in time-varying conditions where traditional methods often fail to detect subtle, evolving damage patterns.

Case Study: Aventa AV-7 Dataset

This research utilizes data from the Aventa AV-7 [13], a 7 kW wind turbine operated by ETH Zurich (Figure 1), which has been monitored to evaluate SHM methods as the turbine approaches the end of its design life. Since 2020, sensors have

Fig. 1 Aventa AV-7 [13].

been deployed throughout the turbine to facilitate system identification, modal analysis, and failure detection studies, with data collected under four specific operational scenarios: normal operation, pitch system failure, aerodynamic imbalance, and rotor icing. For each condition, datasets include time series measurements recorded over specified dates between 2022 and 2023.

The Aventa AV-7 turbine operates with a variable-speed, variable-pitch control, beginning energy generation at a 2 m/s wind speed and ceasing at 14 m/s for a rated power of 7 kW. It has a three-blade rotor with a 12.9 m diameter, positioned 18 m above ground on a concrete and steel tower. A belt-driven generator and a frequency converter enable variable-speed operation.

The turbine is outfitted with eleven accelerometers distributed along the tower, nacelle, main bearing, and generator, as well as two full-bridge strain gauges at the tower base for measuring axial and bending strains. All data is recorded at 200 Hz, while SCADA (Supervisory Control and Data Acquisition) data, such as wind speed, rotor speed, and power output, is recorded at 7 Hz, with temperature and humidity recorded at 1 Hz. The accelerometers are paired and located at specific tower sections to capture the x- and y-axis accelerations aligned with wind direction, allowing comprehensive monitoring of the turbine's structural response.

The SCADA system provides insights into power, wind speed, rotor speed, and yaw angle, which are critical for analyzing turbine performance, especially under ”normal operation” conditions. The power curve, derived from these SCADA readings, illustrates the relationship between wind speed and power output, with distinct operational regions (cut-in, rated, and cut-off speeds) [14].

The dataset further captures three specific fault conditions, providing valuable data for condition monitoring methods.

In February 2022, a failure occurred in the flexible coupling of the pitch drive system, which is critical for adjusting blade angles to optimize performance under changing wind conditions. SCADA data captured deviations in rotor speed, power output, and yaw position compared to normal operation. Before the complete failure, the pitch system became stuck, reducing the turbine's output to 1-2 kW while the rotor speed dropped to around 40 rpm. An emergency stop was triggered to prevent further damage, as indicated by sharp changes in SCADA measurements at approximately 270 seconds. Acceleration data from sensors across the tower and nacelle show a significant structural response to the failure, highlighting its impact on the turbine's dynamics.

In December 2022, rotor icing caused a near-complete halt in turbine operations, reducing rotor speed to almost zero and stopping power generation. This highlights the importance of early detection in cold climates where ice accumulation can significantly reduce aerodynamic efficiency and increase vibration.

Then, data collected after roughness tape was applied to one blade in December 2022 revealed imbalances that affected rotor speed and induced mechanical stress on key turbine components, underscoring the need to identify imbalances early to prevent failures.

This research focuses on the pitch drive failure, as it represents a sudden and critical rupture in the turbine's system. This abrupt failure is particularly challenging for SHM due to the need for immediate detection and intervention to prevent further damage. By concentrating on this sudden event, the study aims to improve SHM techniques' ability to quickly identify and respond to rapid, unforeseen failures, which are often more difficult to manage than gradual damage.

Analysis

The proposed methodology consists of a two-step feature extraction and clustering approach designed to identify structural damage in the turbine system. First, cepstral coefficients are extracted from the system's acceleration time history, providing a compact and computationally efficient representation of the frequency content, which is sensitive to changes in dynamic response caused by damage. Next, image-based features are derived using Gramian Angular Fields, which transform time-series data into two-dimensional images, preserving temporal correlations.

These two types of features are then combined into a unified feature set by applying Principal Component Analysis to reduce dimensionality while retaining the most significant components. Finally, the reduced feature set is analyzed through hierarchical clustering, which groups the data based on similarities in spectral and temporal patterns. This process identifies distinct clusters corresponding to different health conditions, allowing for the detection and classification of damage across various regions of the turbine's operational data.

Cepstral Coefficients

Cepstral coefficients are obtained by applying the Inverse Discrete Fourier Transform (IDFT) to the logarithm of the squared magnitude of a signal's Discrete Fourier Transform (DFT). In the context of SHM, the available signals are typically the system's displacement or acceleration time histories. Accordingly, a set of D cepstral coefficients is defined as follows:

$$CC[q] = \mathcal{F}^{-1}\{\log(|\mathcal{F}\{x[n]\}|^2)\}, \quad q = 0, \ldots, D-1 \tag{1}$$

where $\mathcal{F}$ and $\mathcal{F}^{-1}$ denote the DFT and IDFT, respectively, and $x[n](n = 0, \ldots, N_a - 1)$ represents the discrete acceleration time history of the system under investigation. The selection criterion for the number of cepstral coefficients (D) and its impact on classification performance is detailed in [15].

Examining the formulation of cepstral coefficients reveals their benefits for system representation. The extraction process is both compact and computationally efficient, making it suitable for real-time monitoring and large-scale applications. Additionally, it requires minimal user input, as the only decision involves selecting the number of coefficients (D), reducing the level of expertise needed.

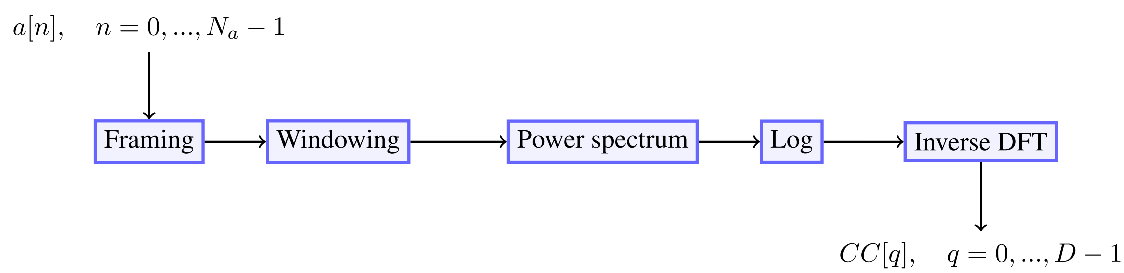

Fig. 2 Cepstral coefficients extraction procedure.

The extraction process follows five key steps, as depicted in Figure 2. Beginning with the system's acceleration time history $x[n]$, the signal is divided into equal-length frames during the framing phase. Each frame is multiplied by a Hamming window to mitigate edge effects (windowing phase). Afterward, D cepstral coefficients are computed for each frame by calculating the power spectrum and applying the logarithm, following Equation 1. Typically, the first coefficient is omitted due to its sensitivity to external forces and sensor noise.

Breaking down the extraction process reveals an additional advantage of cepstral coefficients: their ability to be extracted from small portions of the signal independently. This allows for the sequential analysis of small frames, enabling the description of the system's evolution over time, even in non-stationary signals or complex dynamics. This feature enhances the applicability of cepstral coefficients for analyzing systems characterized by time-varying dynamics.

When structural damage occurs, it alters the system's properties, which leads to changes in its dynamic response. Cepstral coefficients can capture these changes by analyzing the spectral content of the acceleration signal. However, relating specific changes in structural properties to variations in the cepstral coefficients can be challenging, particularly for complex systems.

The analytical formulation presented in [15] clarifies this connection. For an N-degree-of-freedom system subjected to a generic input excitation, the q-th cepstral coefficient ($q > 0$) for the acceleration at the i-th degree of freedom is given by:

$$CC_i[q] = \theta[q] + \gamma_i[q] \tag{2}$$

where,

$$\begin{cases} \theta[q] = \frac{1}{q}\left[\sum_{l=1}^{N} 2e^{-\xi_l \omega_l \Delta T q} \cos \omega_{d,l} \Delta T q - 1\right] \\ \gamma_i[q] = \frac{1}{q}\left[-\sum_{l=1}^{2N-1} {Z'}_l^{(i)q}\right] \end{cases} \tag{3}$$

In these equations, ΔT represents the sampling time, ω and ω_d are the undamped and damped natural frequencies, ξ is the damping ratio, and ${Z'}_l^{(i)q}$ are the roots of a polynomial equation that incorporates both the system's structural properties and the input excitation. While this formulation is straightforward for single-degree-of-freedom systems, it becomes more complex for multi-degree systems, as demonstrated in [15].

Nonetheless, this formulation clarifies that the cepstral coefficients have two main components: $\theta[q]$, which is linked directly to the system's natural frequencies and damping ratios, and $\gamma_i[q]$, which also depends on factors such as input excitation and sensor location.

Image-Based Features

This section extracts image-based features from the acceleration window frames used to extract the cepstral coefficients. The first step consists of encoding the time series as images using the Gramian Angular Field [16], representing time series data in a polar coordinate system instead of the conventional Cartesian coordinates. This approach provides a unique method for capturing the temporal patterns of the data, as each value is mapped to an angular coordinate, while time is represented by the radial coordinate [17, 18].

Given a time series $x[n](n = 0, \ldots, N_a - 1)$, the first step is to rescale the values so that they fall within a fixed range, typically $[-1, 1]$ or $[0, 1]$:

$$\tilde{x}^i_{-1} = \frac{(x_i - \max(X)) + (x_i - \min(X))}{\max(X) - \min(X)} - 1, \qquad \text{or} \qquad \tilde{x}^i_0 = \frac{x_i - \min(X)}{\max(X) - \min(X)} \tag{4}$$

Next, the rescaled time series is transformed into polar coordinates ($\tilde{X}$), where the time values are mapped as radial components and the rescaled values as angular components:

$$\begin{cases} \phi = \arccos(\tilde{x}_i), & -1 \leq \tilde{x}_i \leq 1, \tilde{x}_i \in \tilde{X} \\ r = \frac{t_i}{N_a}, & t_i \in N_a \end{cases} \tag{5}$$

where t_i represents the time stamp, and N_a is a constant factor that regularizes the polar coordinate space. This transformation offers a novel way to interpret time series data by warping values across a range of angles, with the polar coordinate representation preserving the absolute temporal order of the data.

Once transformed, we can compute temporal correlations between different time points by exploiting trigonometric functions. The Gramian Summation Angular Field (GASF) and Gramian Difference Angular Field (GADF) are defined as follows:

$$\text{GASF} = [\cos(\phi_i + \phi_j)] = \tilde{X}' \cdot \tilde{X} - \sqrt{I - \tilde{X}'^2} \cdot \sqrt{I - \tilde{X}^2}^\top \tag{6}$$

$$\text{GADF} = [\sin(\phi_i - \phi_j)] = \tilde{X} \cdot \sqrt{I - \tilde{X}'^2} - \tilde{X}' \cdot \sqrt{I - \tilde{X}^2}^\top \tag{7}$$

where I is the unit row vector $[1, 1, \ldots, 1]$. After converting the time series into polar coordinates, each time step is treated as a one-dimensional metric space, where the inner product between two points x and y is defined as follows:

$$\langle x, y \rangle = x \cdot y - \sqrt{1 - x^2} \cdot \sqrt{1 - y^2}, \qquad \text{or} \qquad \langle x, y \rangle = \sqrt{1 - x^2} \cdot y - \sqrt{1 - y^2} \cdot x \tag{8}$$

This process results in two types of Gramian Angular Fields, GASF and GADF, which can be viewed as quasi-Gramian matrices.

$$G = \begin{bmatrix} \langle x_1, x_1 \rangle & \ldots & \langle x_1, x_n \rangle \\ \vdots & \ddots & \vdots \\ \langle x_n, x_1 \rangle & \ldots & \langle x_n, x_n \rangle \end{bmatrix} \tag{9}$$

The GAFs offer several advantages. First, they maintain temporal dependencies as time progresses from the top-left to the bottom-right of the matrix. Each matrix element $G_{i,j}$ represents the relative correlation between two-time points, determined by the summation or difference of angular values for the corresponding time interval k. The main diagonal $G_{i,i}$, which corresponds to the case when $k = 0$, retains the original value or angular information. This diagonal can be used to reconstruct the original time series from high-level features extracted by deep learning models [16].

After generating these Gramian matrices, they are converted into images for further processing.

The next step involves extracting features from these images using DenseNet [19], a deep convolutional neural network architecture with a unique connectivity pattern. In DenseNet, each layer is connected to all preceding layers within a dense block, allowing each layer to access the feature maps of all previous layers. This dense connectivity facilitates feature reuse and supports efficient gradient flow, leading to a compact model less prone to overfitting [20]. Additionally, DenseNet enables direct supervision of each layer through shortcut connections, enhancing the model's ability to capture detailed pixel-level information without requiring extensive preprocessing [20]. The feature extraction process in DenseNet is particularly suited for capturing the complex patterns within these time series-based images.

Features Fusion and Clustering

This study utilized a combination of cepstral coefficients and image-based features to capture both the spectral and temporal dynamics of the system's vibration signals. Cepstral coefficients provide a concise representation of the frequency content in the signals, while GADF and GASF features convert time-series data into two-dimensional images, preserving temporal relationships between data points. This dual-feature approach allows for a more comprehensive analysis, as it integrates the frequency-domain insights of cepstral coefficients with the temporal correlations encoded by the image-based features.

Once these features were extracted for each time window, Principal Component Analysis (PCA) [21] was applied to reduce the dimensionality of the combined feature set. PCA efficiently selects the most significant components, reducing the complexity of the data while retaining the essential features that contribute most to variance within the dataset. The unified feature set obtained from this dimensionality reduction step is thus optimized for further analysis, making the dataset manageable while still capturing the critical information necessary for detecting and classifying damage.

The next step in the methodology involved applying unsupervised clustering to the reduced feature set in order to identify distinct damage conditions without prior labeling. Clustering was used to group the data based on shared characteristics. This clustering approach is crucial for understanding how the system responds to different types of damage, particularly in complex and evolving environments [22].

Hierarchical clustering was chosen as the primary technique for this task, as it is well-suited for exploratory data analysis and allows for the visualization of relationships between data points in the form of a dendrogram. The hierarchical clustering algorithm works by initially treating each data point as its own individual cluster. At each iteration, the two most similar clusters are merged, progressively reducing the number of clusters until all points are grouped into a single large cluster. This iterative process produces a tree-like structure, which can be ”cut” at different levels to reveal distinct clusters that represent different damage states [23].

The process of hierarchical clustering involves three key steps: (1) calculating the similarity between each pair of objects, (2) linking the objects into a hierarchical tree structure based on these similarities, and (3) determining an appropriate level to ”cut” the dendrogram to define distinct clusters. In this analysis, Euclidean distance was used as the measure of similarity between clusters, ensuring that the clustering process captured both the spectral and temporal characteristics of the data [22].

A notable advantage of hierarchical clustering is its deterministic nature and its ability to provide a clear method for selecting the final number of clusters based on the hierarchical tree structure. However, a significant drawback of this approach is its computational intensity, especially when dealing with large datasets, since the similarity between every pair of objects must be calculated [24]. Despite this, hierarchical clustering was chosen due to its ability to reveal the underlying structure of the data and its effectiveness in grouping complex, high-dimensional data into meaningful clusters that correspond to different damage conditions.

Results

This study was conducted to analyze the pitch drive failure case, which is a mechanism that can be considered developing in three regions, as shown in Figure 3. Initially, the turbine operated under normal conditions, classified as the undamaged case, where rotor speed, wind speed, and power output were stable. A significant decrease in rotor speed and power was observed in damaged region 1, marking the onset of the pitch system failure. Notably, the wind speed remained steady, highlighting that mechanical failure rather than external factors caused the performance degradation. Following this, the pitch system became stuck in an incorrect position, leading to severely reduced power generation (down to nearly 0 kW) despite the rotor continuing to rotate at a lower RPM, identified as damaged region 2. Again, wind speed remained consistent, emphasizing that the turbine's inability to generate power was due to internal failure. Ultimately, the system performed an emergency stop to prevent further damage, labeled as damaged region 3.

The rupture in the pitch drive system limits the turbine's ability to produce adequate power relative to wind speed, significantly affecting the structure's dynamic response. The pitch drive typically adjusts blade angles for optimal performance, but its failure leads to a mismatch between mechanical forces and operational demands. This misalignment alters load distribution and reduces the effective stiffness, particularly in the drivetrain and support structures. As stiffness decreases, the natural frequencies drop, making the structure less resistant to dynamic loads. In the damaged regions, the cepstral analysis shows irregular frequency content, with lower-frequency components dominating, reflecting the structural degradation and stiffness loss caused by the pitch failure.

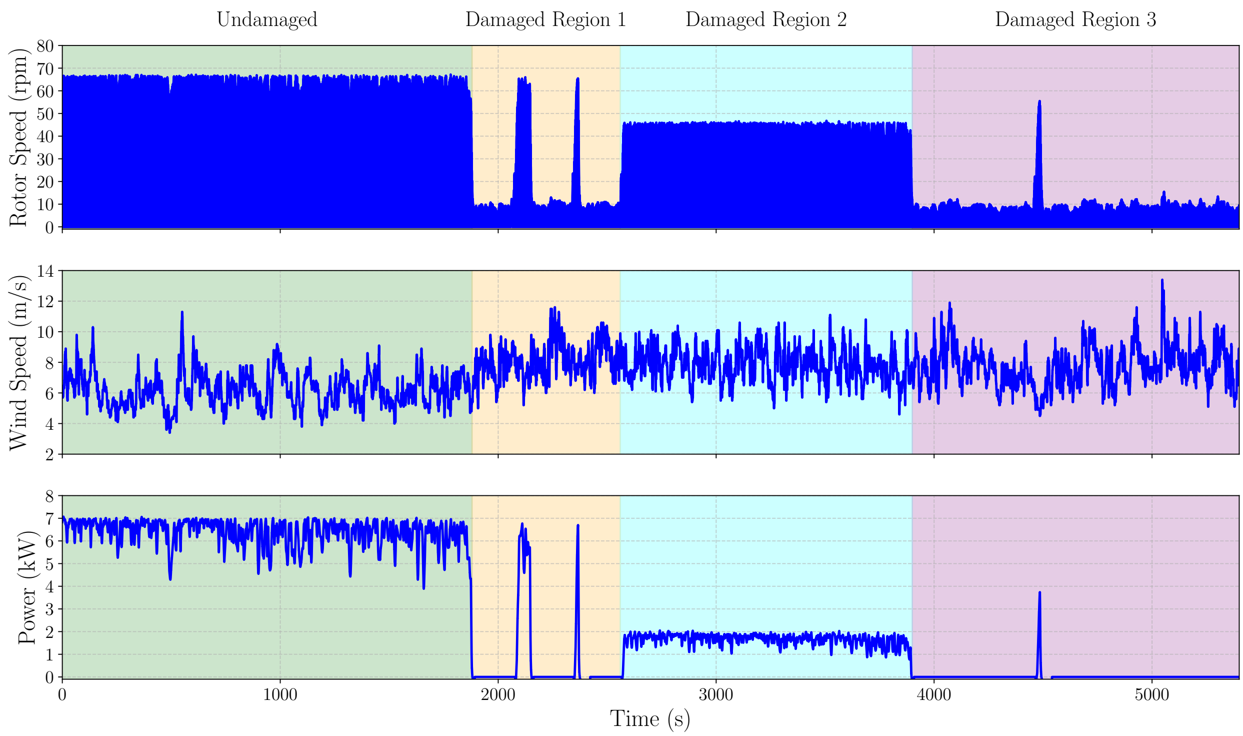

Fig. 3 Progression of turbine operational states from normal to pitch failure across identified damage regions.

Figure 4 illustrates the variation of cepstral coefficients across the turbine's operational states, focusing on how the pitch drive failure affects the system's dynamic response. After discarding the first cepstral coefficient, the remaining coefficients provide insights into the structural changes occurring due to the failure. The lower-order coefficients (second, third, etc.) show noticeable deviations as the damage progresses, particularly in damaged region 1, where the smoothness seen in the undamaged state begins to break down. This reflects significant structural changes, as these coefficients are sensitive to shifts in the system's primary spectral content, such as changes in natural frequencies or damping. As the failure worsens in damaged region 2, the higher-order coefficients become increasingly irregular, capturing finer details of the dynamic response and reflecting more complex, nonlinear effects caused by the pitch failure. The growing irregularity across both lower- and higher-order coefficients highlights the progressive degradation of the system, with lower-order coefficients capturing broad structural changes and higher-order coefficients revealing more detailed variations in the frequency content. Together, these changes provide a comprehensive picture of the system's instability as the pitch drive failure progresses.

The GADF and GASF images across various regions in Figure 5 illustrate how pitch drive failure influences temporal dynamics correlations. The fusion of GADF and GASF images facilitates the capture of both global patterns and localized fluctuations, as GADF accentuates time-series anomalies, while GASF emphasizes collective behavioral trends within the data [11]. The images for undamaged regions reveal higher rotor speeds, consistent with stable operational behavior. Conversely, in damaged regions 1 and 3, where rotor speeds are lower, distinct deviations in image patterns can be observed, indicative of impaired functionality. Damaged region 2 displays characteristics suggestive of malfunction, though with distinct features differing from regions 1 and 3, highlighting specific anomalies in rotor speed that further underscore varying degrees of pitch drive impairment.

After extracting cepstral coefficients and image-based features, the two sets of features were fused as previously described. Initially, the individual features were subjected to PCA to reduce dimensionality, with only the major components retained to form a combined feature set. This unified feature set was then used as input to the hierarchical clustering algorithm. The resulting dendrogram, displayed in Figure 6, illustrates the hierarchical grouping of samples, where each node represents the merging of clusters based on their similarity. Along the x-axis, the distance between clusters is shown, which reflects the level of similarity across samples within each group.

Based on the dendrogram, three clusters were selected to categorize the dataset. The merged features were thus organized according to these three clusters, as illustrated in Figure 7. Here, rotor speed and acceleration data are color-coded based on their cluster assignments, clearly distinguishing damaged states from undamaged ones. Notably, damage regions 1 and 3 are

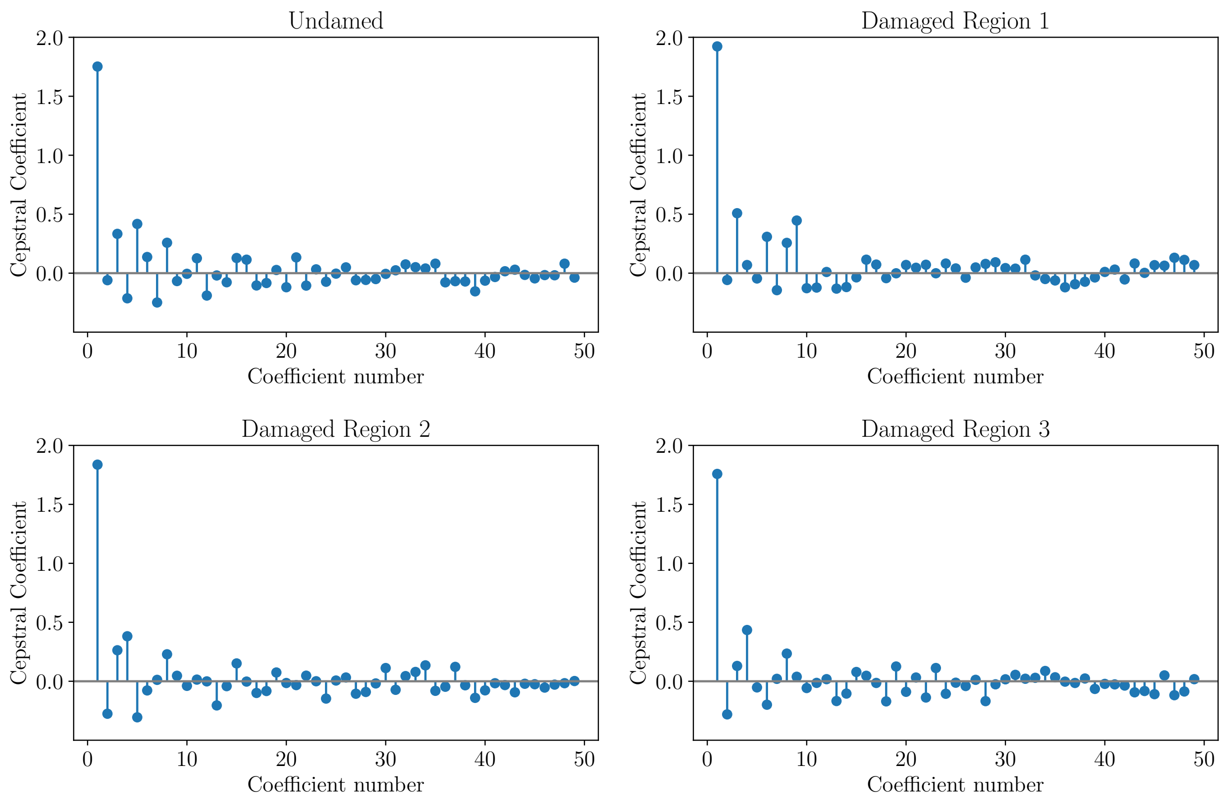

Fig. 4 Sample cepstral coefficient variations across regions of pitch drive failure.

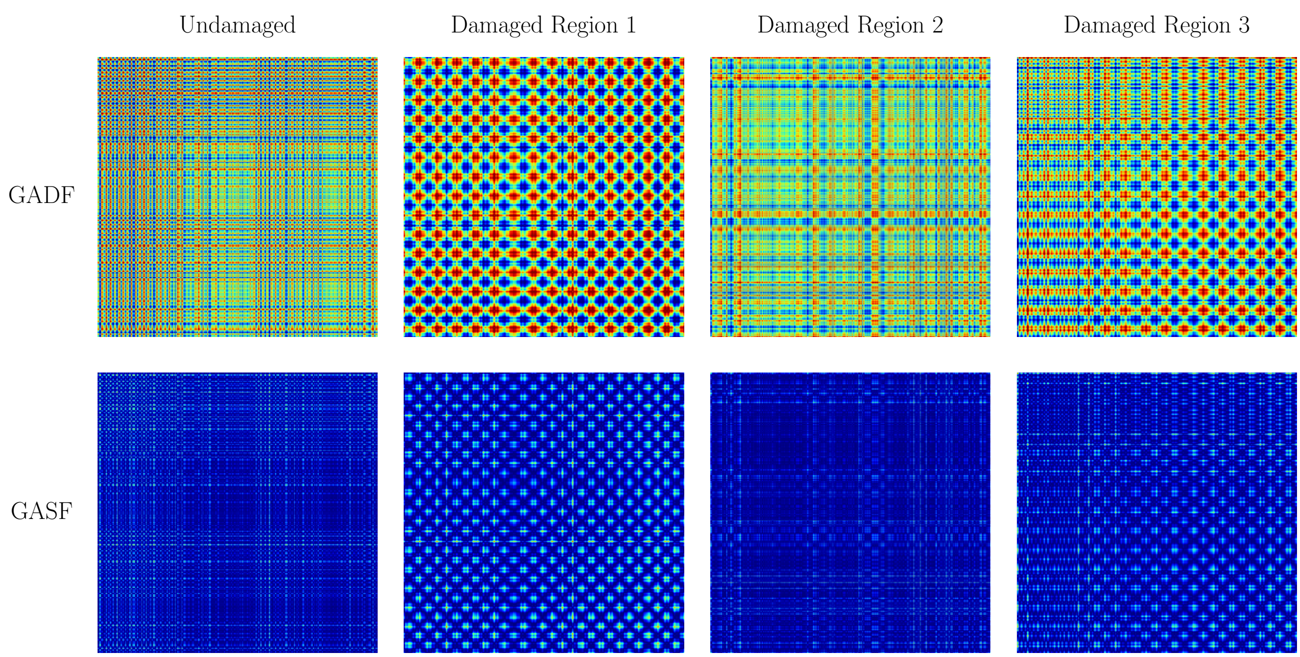

Fig. 5 Sample GAF image variations across regions with pitch drive failure.

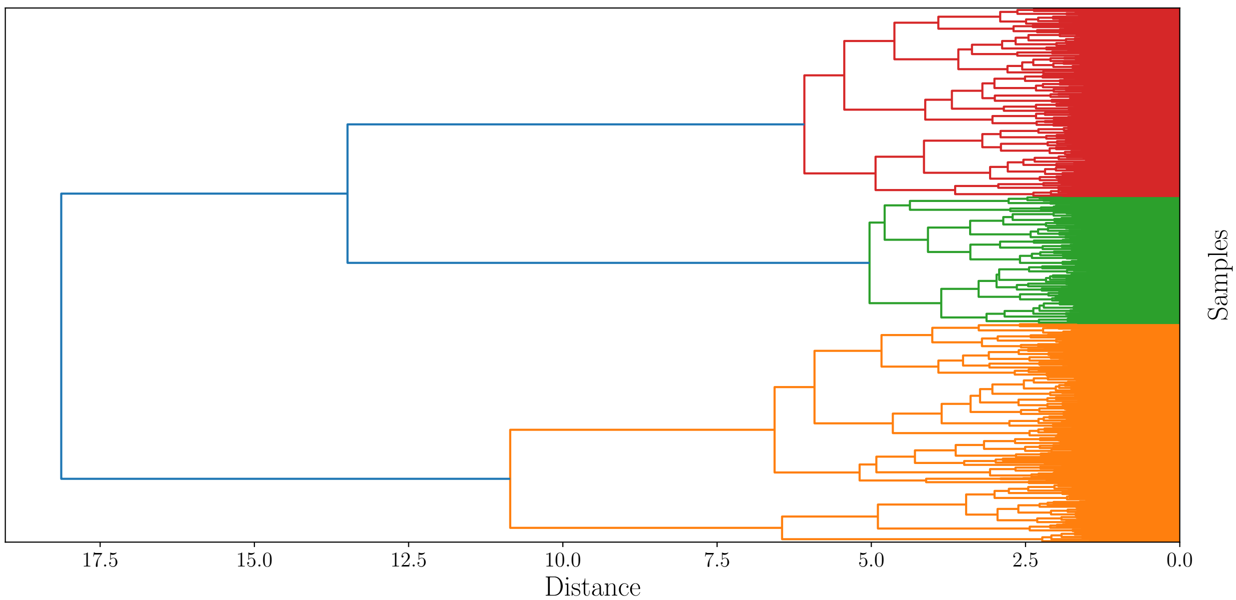

Fig. 6 Dendrogram showing hierarchical clustering of pitch drive failure time-series samples over time.

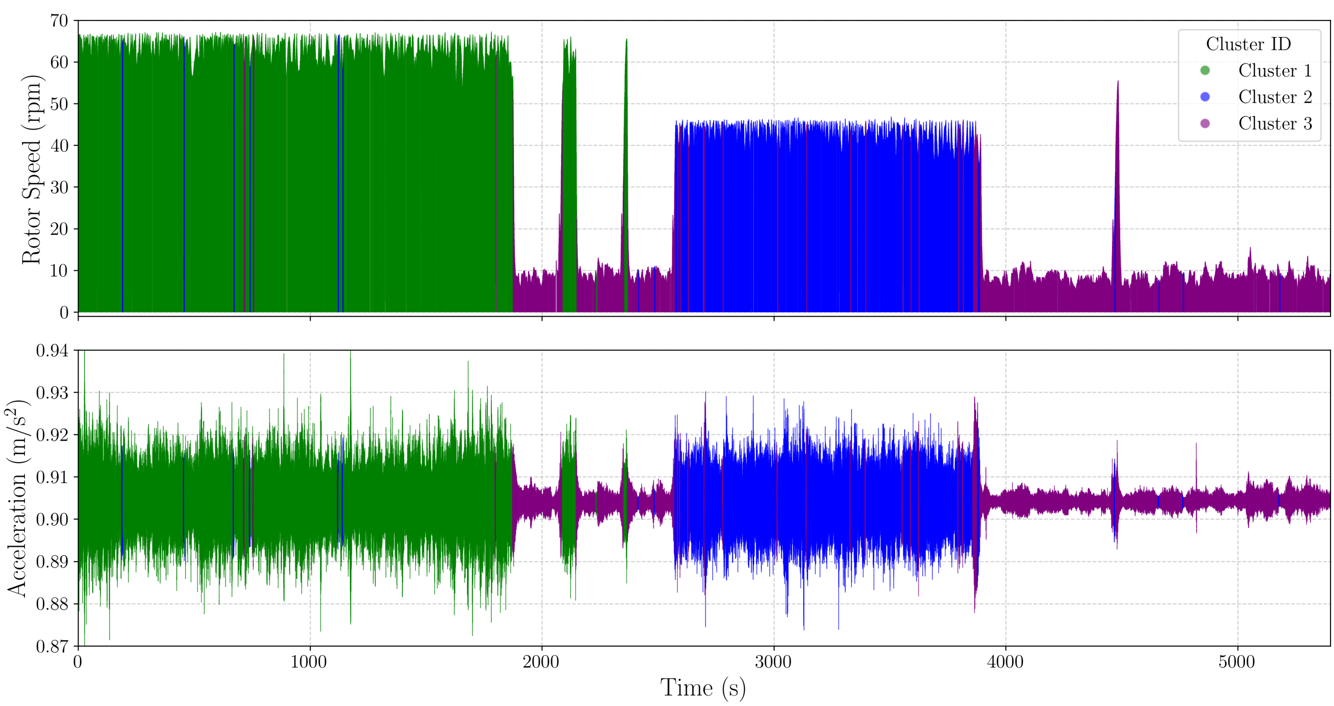

Fig. 7 Clustered rotor speed and acceleration, distinguishing damaged from undamaged states.

grouped into the same cluster, indicating shared dynamic characteristics between these regions. However, region 2, exhibiting a higher rotor speed than regions 1 and 3, is distinctly clustered, underscoring the influence of different operational dynamics on damage classification.

Conclusion

In conclusion, this study presents an integrated framework for damage identification in dynamic structural systems by combining cepstral and time-image-based features. The application of cepstral coefficients, originally from the field of speech recognition, enables effective tracking of frequency content changes, providing a robust foundation for identifying stationary and nonstationary DSFs. However, due to limitations in capturing fine-grained temporal dynamics, these coefficients were augmented with GAF transformations, which allow time series data to be visualized and analyzed as images. This dual-feature approach not only enhances damage detection accuracy but also allows for the precise localization of evolving structural damage.

The methodology was tested on the Aventa AV-7 wind turbine dataset, particularly focusing on the pitch drive failure scenario, which demonstrated significant degradation of the system's frequency response. This approach successfully classified distinct damage states through hierarchical clustering, validating the framework's capacity to capture complex, time-evolving structural behaviors. These results indicate that a more adaptive and comprehensive solution for SHM applications in dynamic environments is achievable by merging cepstral and image-based analysis.

Acknowledgments The authors would like to sincerely thank ETH Zurich and its collaborators for providing the "Aventa AV-7" dataset, which was invaluable for our study.

References

1. Fan, W. and Qiao, P. "Vibration-based damage identification methods: a review and comparative study". *Structural health monitoring*, 10(1):83–111 (2011)
2. Hou, R. and Xia, Y. "Review on the new development of vibration-based damage identification for civil engineering structures: 2010–2019". *Journal of Sound and Vibration*, 491:115741 (2021)
3. Farrar, C.R. and Worden, K. "An introduction to structural health monitoring". *Philosophical Transactions of the Royal Society A: Mathematical, Physical and Engineering Sciences*, 365(1851):303–315 (2007)
4. Farrar, C.R. and Worden, K. *Structural health monitoring: a machine learning perspective*. John Wiley & Sons (2012)
5. Abasi, A. and Sadhu, A. "Performance evaluation of blind modal identification in large-scale civil infrastructure". *Infrastructures*, 7(8):98 (2022)
6. Moughty, J.J. and Casas, J.R. "A state of the art review of modal-based damage detection in bridges: Development, challenges, and solutions". *Applied Sciences*, 7(5):510 (2017)
7. Tronci, E.M., De Angelis, M., Betti, R., and Altomare, V. "Multi-stage semi-automated methodology for modal parameters estimation adopting parametric system identification algorithms". *Mechanical Systems and Signal Processing*, 165:108317. Elsevier (2022)
8. Tronci, E.M., Beigi, H., Betti, R., and Feng, M.Q. "A damage assessment methodology for structural systems using transfer learning from the audio domain". *Mechanical Systems and Signal Processing*, 195:110286 (2023)
9. Li, L., Morgantini, M., and Betti, R. "Structural damage assessment through a new generalized autoencoder with features in the quefrency domain". *Mechanical Systems and Signal Processing*, 184:109713 (2023)
10. Wu, T., Cheng, X., Yan, Z., Yang, J., Chai, X., and Dai, X. "Acoustic tunnel lining cavity detection using cepstral coefficients with optimized filter bank". *Measurement Science and Technology*, 35(6):066115 (2024)
11. Si, Y., Zhu, D., Chen, Y., Liu, J., Chen, T., and Dong, Z. "Prediction of brown tide algae using improved gramian angular field and deep learning based on laser-induced fluorescence spectrum". *Measurement Science and Technology*, 34(9):095501 (2023)
12. Gonen, S. and Erduran, E. "A hybrid method for vibration-based bridge damage detection". *Remote Sensing*, 14(23):6054 (2022)
13. Chatzi, E., Abdallah, I., Hofsäß, M., Bischoff, O., Barber, S., and Marykovskiy, Y. "Aventa AV-7 ETH Zurich Research Wind Turbine SCADA and high frequency Structural Health Monitoring (SHM) data" (2023)
14. Bilendo, F., Meyer, A., Badihi, H., Lu, N., Cambron, P., and Jiang, B. "Applications and modeling techniques of wind turbine power curve for wind farms—a review". *Energies*, 16(1):180 (2022)
15. M.Morgantini, R.Betti, and L.Balsamo. "Structural damage assessment through features in quefrency domain". *Mechanical Systems and Signal Processing*, 147:107017 (2021)
16. Wang, Z. and Oates, T. "Imaging time-series to improve classification and imputation". *arXiv preprint arXiv:1506.00327* (2015)
17. Wu, Q., Li, Y., Ouyang, H., and Xuan, Y. "A multimodal fusion human activity recognition method based on cnn and gramian angular field". In *Third International Conference on Advanced Algorithms and Neural Networks (AANN 2023)*, volume 12791, pages 368–373. SPIE (2023)
18. Xu, H., Li, J., Yuan, H., Liu, Q., Fan, S., Li, T., and Sun, X. "Human activity recognition based on gramian angular field and deep convolutional neural network". *IEEE Access*, 8:199393–199405 (2020)
19. Zhu, Y. and Newsam, S. "Densenet for dense flow". In *2017 IEEE international conference on image processing (ICIP)*, pages 790–794. IEEE (2017)
20. Jiang, W., Zhang, D., Ling, L., and Lin, R. "Time series classification based on image transformation using feature fusion strategy". *Neural Processing Letters*, 54(5):3727–3748 (2022)
21. Abdi, H. and Williams, L.J. "Principal component analysis". *Wiley interdisciplinary reviews: computational statistics*, 2(4):433–459 (2010)
22. Hair, J., Anderson, R., Tatham, R., and Black, W. "Multivariate date analysis.(prentice-hall, englewood cliffs, nj)" (1998)
23. Nielsen, F. and Nielsen, F. "Hierarchical clustering". *Introduction to HPC with MPI for Data Science*, pages 195–211 (2016)

24. Magalhães, F., Cunha, A., and Caetano, E. "Online automatic identification of the modal parameters of a long span arch bridge". *Mechanical Systems and Signal Processing*, 23(2):316–329 (2009)